Solid Freeform Fabrication 2024: Proceedings of the 35th Annual International Solid Freeform Fabrication Symposium – An Additive Manufacturing Conference
Reviewed Paper

Design and Fabrication of a Micro-nozzle for Aerosol Jet Printing

[1]Md Shihab Shakur, [2]Md Nazmus Sakib, [1]Erik Inman, [1]Srikanthan Ramesh
[1] School of Industrial Engineering and Management, Oklahoma State University, Stillwater, OK 74078, USA.
[2] School of Mechanical and Aerospace Engineering, Oklahoma State University, Stillwater, OK 74078, USA.

Abstract

Aerosol jet printing is a micro-scale additive manufacturing technique that involves the deposition of a polydisperse stream of aerosol through a converging nozzle. Typically, the smaller droplets in the aerosol stream tend to expand along with the gas flow and deviate from the central axis as soon as they leave the nozzle, leading to a printing defect known as overspray. The study explores the feasibility of using a series of converging-diverging sections integrated into the nozzle to enhance stream collimation, improve print resolution, and minimize the occurrence of overspray. The study discusses these micro-nozzles' design and fabrication and compares their overspray and print resolution performance to commercial nozzles. Preliminary results suggest that the proposed nozzle design is capable of yielding finer lines and reducing overspray by 17.821% at a low focusing ratio and minimal overspray across a range of gas flow parameters. Future work can focus on optimizing the nozzle geometries and conducting a detailed analysis of the effect of nozzle design features on aerosol collimation, stream trajectories, and temporal stability of focusing and deposition.

Keywords
Micro-scale additive manufacturing, process design, functional prototyping, aerosol jet printing, flexible electronics

1. Introduction

Aerosol jet printing (AJP) is an additive manufacturing technique that deposits fine droplets of functional materials onto a substrate by directing an aerosol mist through a nozzle [1]. AJP has traditionally been used to print conductive inks to create electronic circuits, sensors, and other advanced microelectronic applications [2]. Conductive traces as narrow as 10 μm have been achieved using AJP [3], [4], [5]. In AJP, a carrier gas transports the aerosolized ink droplets to a transition region in the printhead, where an annular sheath gas envelops the incoming stream, enabling constriction and collimation [6]. The ideal result of this three-way multiphase fluid interaction is a high-density deposit of aerosol droplets with feature sizes considerably smaller than the typical nozzle diameter (~150-300 μm) [7]. Nevertheless, suboptimal process conditions in the printhead often result in the printed features bearing signs of high edge roughness, material inadequacy, and over-deposition [8].

One of the major issues in AJP is a print defect called overspray, where excess material is deposited outside the intended areas. This defect restricts miniaturization and degrades electrical properties by creating unintended conductive paths and increasing parasitic capacitance in printed microelectronics. Previous studies have shown that smaller aerosol droplets form overspray due to two primary reasons: i) a low Stokes number, which causes the droplets to follow the fluid transport, and ii) a negligible Saffman lift force, leading to weaker collimation towards the nozzle centerline [9]. As a result, these droplets exhibit a greater positional spread between the nozzle exit and the substrate. The expansion of fluid flow exiting the nozzle, combined with these factors,

causes smaller droplets to follow the gas streamlines and experience a high degree of spread beyond the nozzle exit, resulting in overspray.

Previous studies have examined the effect of nozzle design on the collimation of aerosol streams in AJP. The most commonly used designs are convergent nozzles, available as plastic tapered tips or thin wall precision tip nozzles [9]. In a convergent nozzle, the aerosol stream accelerates due to the conservation of mass, requiring an increase in velocity as the cross-sectional area decreases. However, these nozzles often fail to sufficiently accelerate smaller droplets in the polydisperse aerosol stream, which, due to their lower inertia, tend to disperse with the expanding gas flow outside the nozzle. To address this issue, other key process parameters, such as gas flow rates, ink properties, and gas phase saturation, are often modulated [10], [11], [12].

Alternative nozzle geometries build on the principle of increasing aerosol droplet velocity [13]. For instance, convergent-divergent nozzles accelerate aerosol particles in the convergent section and further accelerate them in the divergent section, potentially achieving higher velocities and better collimation [14]. Nonetheless, these nozzles have primarily been applied to dry particles in applications like cold spray [15] and plasma-assisted deposition of non-spherical particles [14], with limited research on their effects on the collimation, acceleration, and deposition of spherical micro-droplets.

This study evaluates the feasibility of using multi-throat converging-diverging (CD) micro-nozzles for the aerosol printing of a conductive ink made of poly(3,4-ethylenedioxythiophene) polystyrene sulfonate (PEDOT: PSS). The performance of the proposed design is assessed through a combination of 3D physics-based numerical modeling and empirical testing. The study outlines with a discussion of the micro-nozzle design and provides a brief overview of the fabrication method utilized. Subsequently, this study examines the effect of nozzle design on the acceleration of aerosol droplets, collimation, and quality metrics of printed features, such as mean line width and percentage of overspray area.

2. Materials

Conductive PEDOT: PSS inks (0.8% in water) were used as received for all printing experiments. The printing experiments were carried out on treated PET substrates from NovaCentrix. PEDOT (poly(3,4-ethylenedioxythiophene) polystyrene sulfonate) is a conductive polymer ink known for its high electrical conductivity and flexibility. Its solution-processable nature facilitates applications in organic electronics, such as flexible displays and sensors [16], [17], [18].

3. Methods

3.1. Design Iterations and Fabrication of Micro-Nozzles

The micro-nozzle, designed in SolidWorks 2022, comprises of three converging sections around a central diverging section and was fabricated using stereolithography (SLA). The initial design faced clogging and resin shrinkage issues, particularly in the narrow converging sections (Figure 1A). In the second iteration (Figure 1B), the diameter of the converging-diverging sections was increased by 0.25mm, and the CD section was repositioned higher to enhance resin flow and reduce clogging. Additionally, the nozzle exit diameter was reduced to address shrinkage, and the model was sliced at a 15° angle to improve resin release and minimize support material in the micro-channels. However, in the second iteration, problems persisted, as the nozzle tip occasionally fractured during the removal of the support material, and there were cases of trapped

resin that caused clogs after curing. In the third iteration (Figure 1C), further refinements were made, such as increasing the outer diameter of the nozzle and integrating a 400 µm pin, similar to standard 22GA tapered tip dispensing nozzles made by the Original Equipment Manufacturer (OEM), to facilitate resin flow and reduce the entrapment of support material. The final design of the multi-throat CD micro-nozzle is shown in Figure 1D. The redesigned nozzle was then fabricated with a Formlab 3 SLA printer, using a bottom-up approach with a layer thickness of 100 µm. After printing, the part underwent 15 minutes of washing with water and 90% isopropyl alcohol to remove residual support material and uncured resin. It was then cured for 10 minutes to ensure material strength and stability.

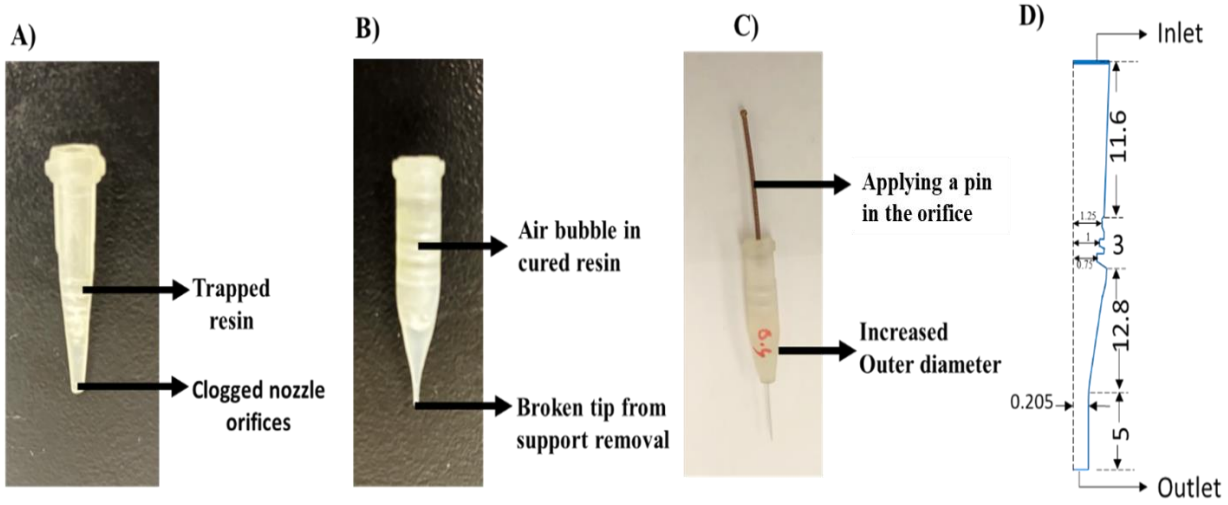

Figure 1. Design iterations of the multi-throat CD nozzles for the AJP, (A) Iteration 1, (B) Iteration 2, (C) Iteration 3, (D) CD nozzle internal geometry with dimensions in mm.

3.2. Numerical Modeling Aerosol Flow through Micro-Nozzles

3D Computational fluid dynamics (CFD) models were developed to evaluate the flow of aerosol droplets through the proposed nozzle design. The flow through the jetting assembly was assumed to be incompressible, and a pressure-based solver in ANSYS fluent was used to estimate key flow variables of the continuous gas phase. ANSYS Fluent is a CFD software widely utilized for simulating fluid flow, heat transfer, and chemical reactions across various engineering domains, including advanced manufacturing [19], [20]. Fluent facilitates the simulation of both single-phase and multiphase flows, encompassing reacting flows, turbulence, acoustics, and even electromagnetics in fluid systems.

In this study, the realizable $k-\in$ model was used to model the aerodynamic interactions in the print channel accurately. The trajectory of the ink droplets was predicted by solving the force balance on each droplet as they moved through the print channel. A Lagrangian discrete phase model (DPM) was used to determine the velocities using a one-way coupling between the particles (droplets) and the fluid (combined gas flow). The sheath gas inlet and carrier gas inlet were defined as velocity inlets. The walls of the print channel and the nozzles were considered stationary walls. The nozzle outlet was specified as a pressure outlet and subjected to an "escape" boundary condition, and the substrate was considered a moving wall for the aerosol droplets to be trapped when they were in contact. Further details of the numerical framework, including the free body diagram of forces acting on aerosol droplets, can be found in our previous publications [6], [9].

3.3. Aerosol Jet Printing

An IDS NanoJet™ printer, illustrated in Figure 2, was used to deposit PEDOT: PSS ink onto a flexible, treated PET substrate. The atomization voltage was set to 36 V. A carrier gas flow rate of 10 standard cubic centimeters per minute (SCCM) was maintained throughout the printing process to ensure consistent transport of the aerosol droplets. The sheath gas flow rate was varied between 40 and 150 SCCM in increments of 10 SCCM. For all printing experiments and simulations, a standard 22G plastic tapered nozzle (ID: 410 µm) was used as a benchmark to compare the performance of the multi-throat CD micro-nozzle. The stage speed was maintained at 3 mm / s, while the stand-off distance (i.e., distance between the nozzle tip and substrate) was maintained at 1.25 mm.

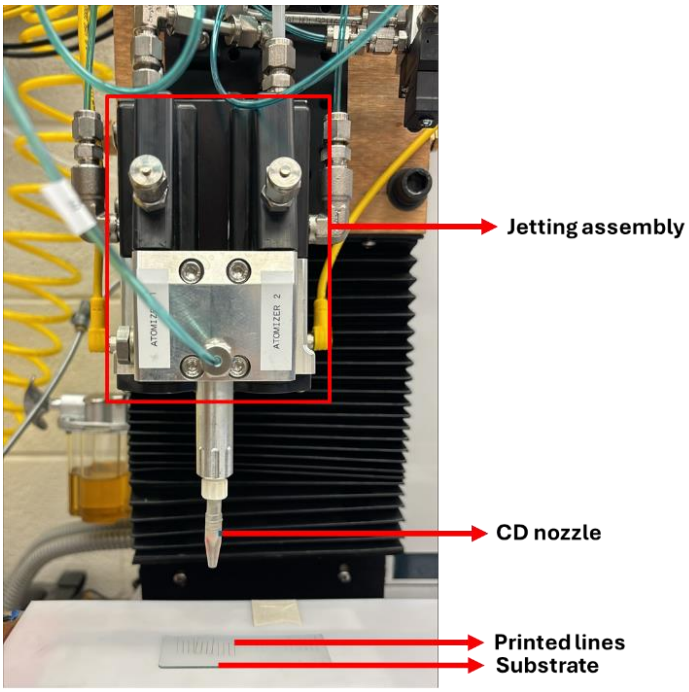

Figure 2: Aerosol Jet printhead with CD nozzle.

3.4. Line Width Measurement

The printed line patterns were examined using optical microscopy (VHX-5000, Keyence, USA) equipped with a high-resolution camera. The microscopy was mainly performed with 500x magnification to capture detailed images. The thickness and cross-sectional area of the printed lines were determined by microscopic analysis. In addition, the line width and height of the printed circuit were measured to evaluate conductivity across the samples. The test samples were multiple lines with a single time pass. The test specimens consisted of 10 mm long lines printed in four consecutive rows, each separated by a 3 mm gap. Each line was printed once to ensure consistency across samples. Three independent samples per test condition were used to obtain line widths, and data are represented as mean $\pm$ SD.

3.5. Overspray Quantification

The printed specimens' images were analyzed for overspray using ImageJ. The raw images were converted to 8-bit binary pixels through thresholding and analyzed with the 'Analyze Particles' tool. Each printed line was treated as a 'super-particle' with a length equal to the number

of pixels in the x-direction (X_{length}) and a width (L_w) calculated as the area of the line (L_A) divided by X_{length}. The center of area coordinates (Y_{center}) and L_w were used to determine the lower (Y_{lower}) and upper (Y_{upper}) edge coordinates of the line. For lines with diffused, Y_{lower} and Y_{upper} were considered as averaged positions, typically corresponding to locations where the particle area coverage was approximately 50%. To assess overspray, the region outside the central line was divided into consecutive strips with a width of $0.1 \times L_w$ and length of X_{length}. Each strip was evaluated to determine the percent area coverage by overspray based on the number of pixels within the strip. This analysis categorized overspray coverage into defined ranges relative to the line width.

3.6. Resistivity Measurement

After printing, the test samples were dried at ambient temperature for 10 minutes, followed by a 30-minute thermal sintering at 165 °C to improve line conductivity. Line dimensions were measured for consistency in width and height, and mean values were calculated. Resistivity measurements were performed with a 2-point probe, as illustrated in Figure 3, taking three readings at specified endpoints. Resistivity (ρ) was determined using Ohm's law as described by Ramon et al. [21].

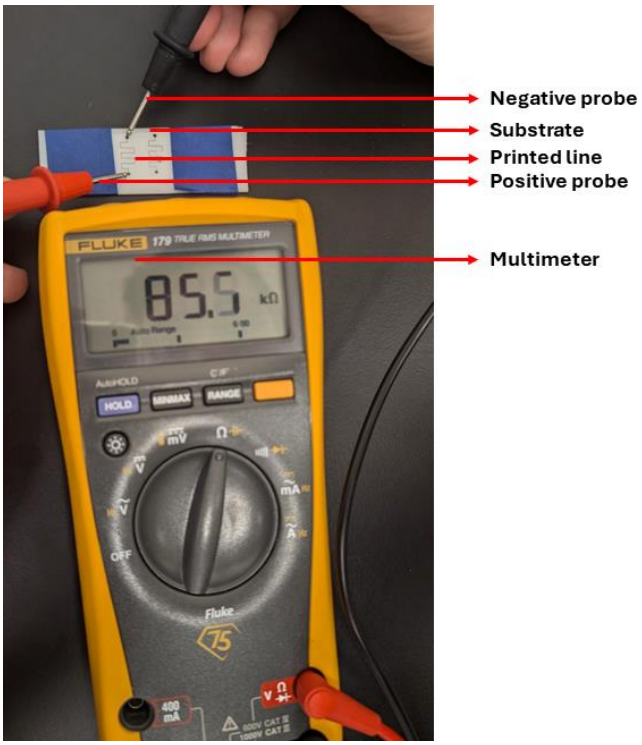

Figure 3: Measuring the resistance of the circuit with a 2-point probe.

4. Results and Discussion

4.1 Nozzle Design and Manufacturing

Figure 4A shows the CAD model of the fabricated multi-throat CD micro-nozzle with three CD sections in series. These CD sections have equal vertical lengths, but the internal channel diameter decreases to facilitate particle collimation. The total length, outer, and inlet diameter at the nozzle exit are consistent with the standard 22G tapered tip nozzle. Each converging section constricts the aerosol jet further, with a half-cone angle of 14° (as shown in Figure 4B). Through

pilot experiments, we observed that angles lower than 14° facilitate nozzle clogging. A cross-section of the SLA-printed part is shown in Figure 4C. Minor dimensional deviations from the nominal design were observed in the SLA-manufactured nozzle, specifically in the half-cone angle (13.7°), the length of the converging section, and the outlet diameter. These deviations are attributed to shrinkage during the curing process. Figure 4D illustrates the fluid domain used for the simulations, featuring the multi-throat CD nozzle attached to the flow cell.

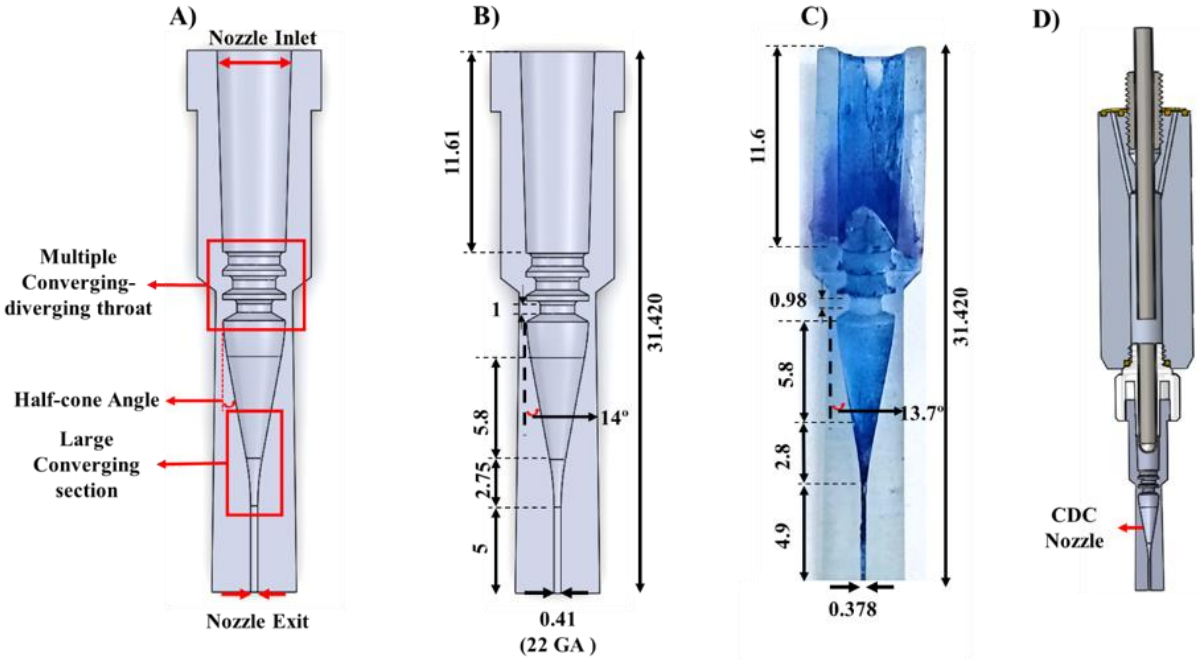

Figure 4. (A) Cross-sectional view of the CAD model of a multi-throat CD micro-nozzle, (B) Key dimensions of the micro-nozzle, (C) Cross-sectional image of an SLA-printed micro-nozzle dyed blue for better visualization, and (D) fluid domain considered for the numerical simulations.

4.2 Numerical Modeling of Aerosol Droplet Velocity

Figure 5 shows CFD-predicted aerosol trajectories and velocities for both OEM (Figure 5A) and multi-throat CD (Figure 5D) micro-nozzles. The sheath gas collimates the aerosol stream more effectively at higher concentration ratios (sheath gas flow to carrier gas flow rate), as seen in the narrower line widths of Figures 5C and 5F (FR of 15) compared to Figures 5B and 5E (FR of 4). A higher exit velocity of the aerosol stream is desirable in AJP. This is because an aerosol stream with a higher velocity will have greater momentum, preventing it from closely following and spreading along with the expanding gas at the nozzle exit. Figure 4 shows that the CFD-predicted results indicate the multi-throat converging-diverging (CD) micro-nozzle generates a higher aerosol exit velocity at a given focusing ratio, defined as the ratio of sheath gas flow rate (SGFR) to carrier gas flow rate (CGFR), compared to the 22G tapered tip nozzle. Consequently, for a given FR, the multi-throat CD micro-nozzle yields a narrower ink stream width than the commercial nozzle, thereby improving print quality, as demonstrated by the micrographs in Figure 5.

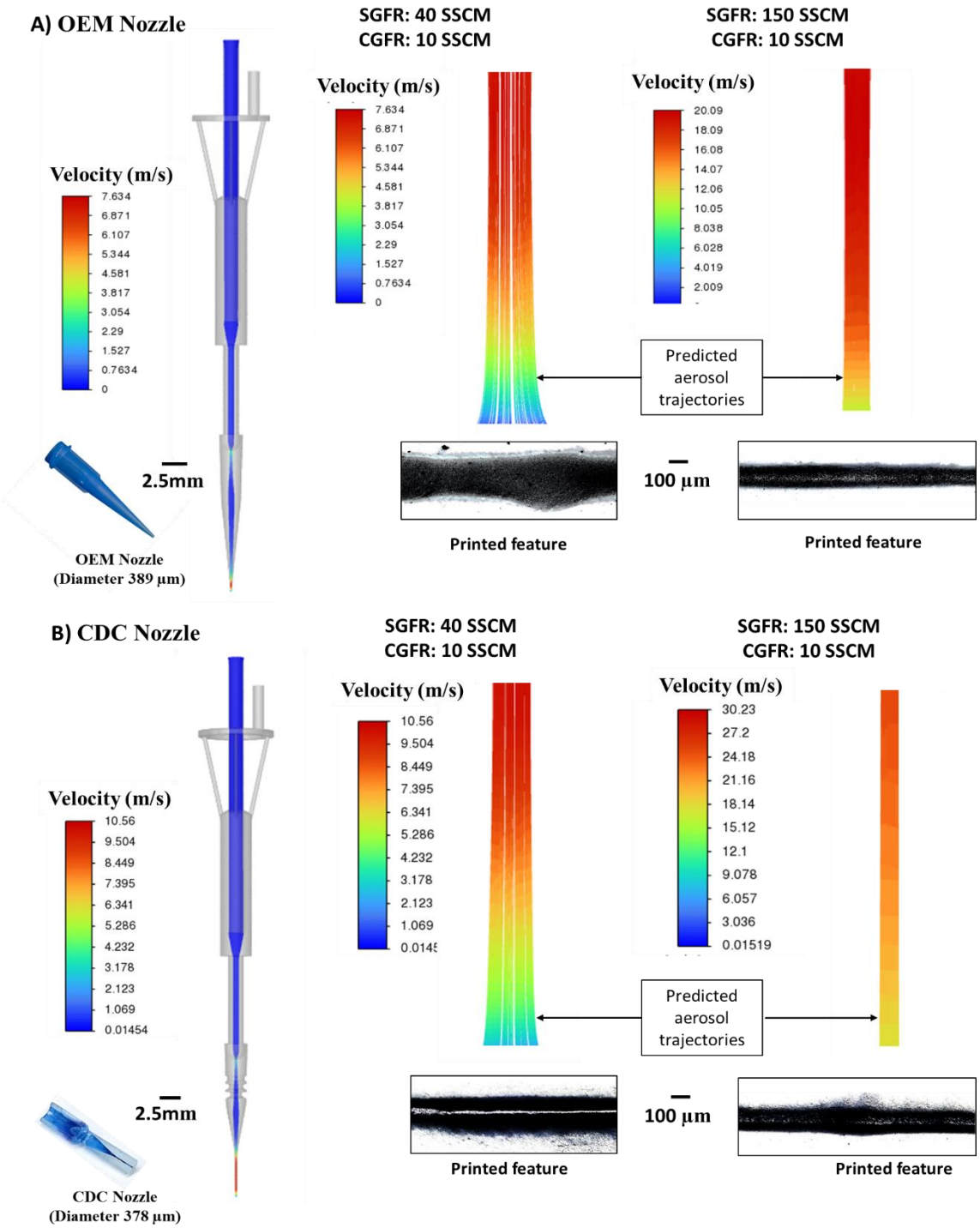

Figure 5. (A) Aerosol trajectory throughout the 22G tapered tip nozzle assembly as predicted by CFD simulation. Stream trajectories from the nozzle exit to the substrate are depicted for the 22G tapered tip nozzle with a CGFR of 10 sccm and SGFRs of (B) 40 sccm and (C) 150 sccm. (D) Aerosol trajectory throughout the CD micro-nozzle assembly as predicted by CFD simulation. stream trajectories from the nozzle exit to the substrate are depicted for the multi-throat CD micro-nozzle with a CGFR of 10 sccm and, SGFRs of (E) 40 sccm, and (F) 150 sccm. The micrographs show the printed features resulting from the corresponding gas flow conditions.

Figure 6 illustrates the difference in line widths between OEM and multi-throat CD micro-nozzles for FR ranging from 4 to 5. As shown, the multi-throat CD micro-nozzle produces a narrower line width for a given FR than the OEM nozzle, which is consistent with our previous discussion. Additionally, it is apparent that the CFD-predicted line widths are smaller than those obtained from experimental measurements of the printed lines. This discrepancy arises from the assumption in the simulation that the particle stream will be trapped immediately upon contact with the substrate. However, in reality, the aerosol stream splashes or bounces back when it hits the substrate, resulting in a wider line width than predicted by the CFD simulations.

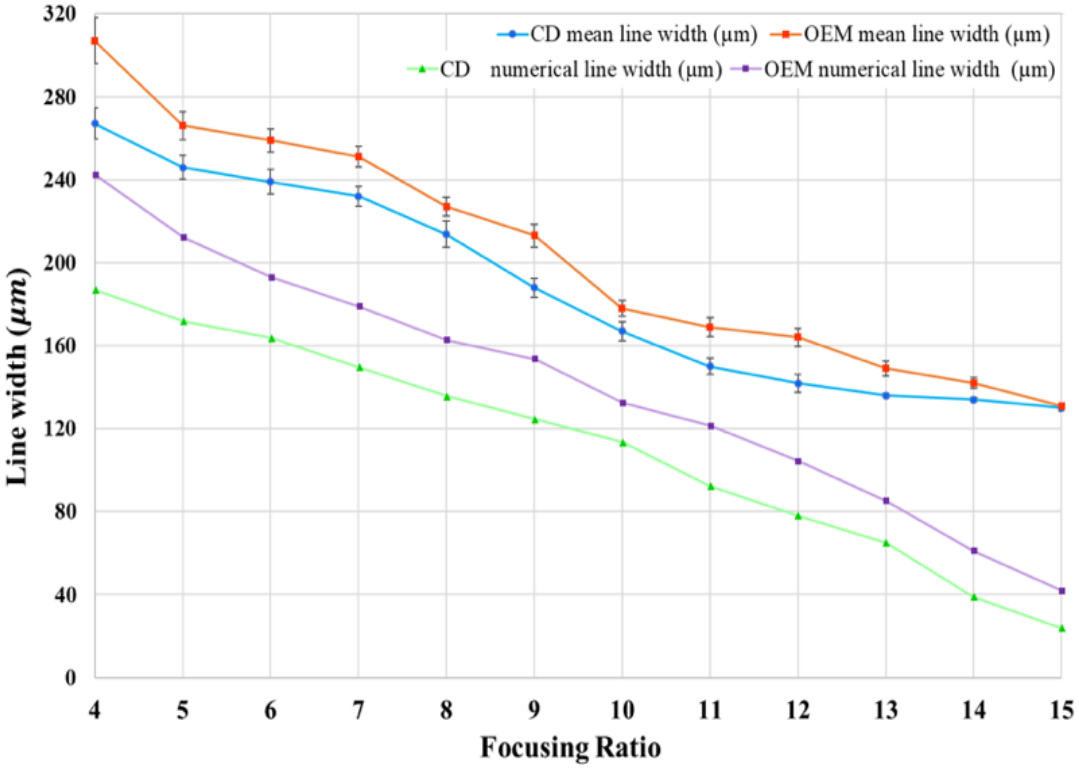

Figure 6. Comparison of multi-throat CD and OEM nozzle line width with respect to focusing ratio.

4.3. Overspray Quantification

Figure 7 illustrates the overspray area as a function of the focusing ratio. It can be seen that irrespective of the nozzle geometry used, overspray decreases with increasing focusing ratio. For the micro-nozzle, overspray sharply decreased from 17.94% at a focusing ratio of 4 to just 0.119% at a focusing ratio of 15. The OEM nozzle also showed a reduction, starting with a higher overspray of 24.552% at a focusing ratio of 4 and decreasing to 0.115% at a focusing ratio of 15. This high overspray at lower focusing ratios is likely due to insufficient sheath gas flow, leading to less confinement and directionality of the aerosol stream. At higher focusing ratios (14-15), both nozzles exhibited similar low overspray percentages, indicating that increased sheath gas flow rates effectively reduce the expansion of smaller droplets once they exit the nozzle. Our results indicate that while the CD micro-nozzle has better performance at lower focusing ratios, both nozzles achieve comparable, minimal overspray at higher focusing ratios.

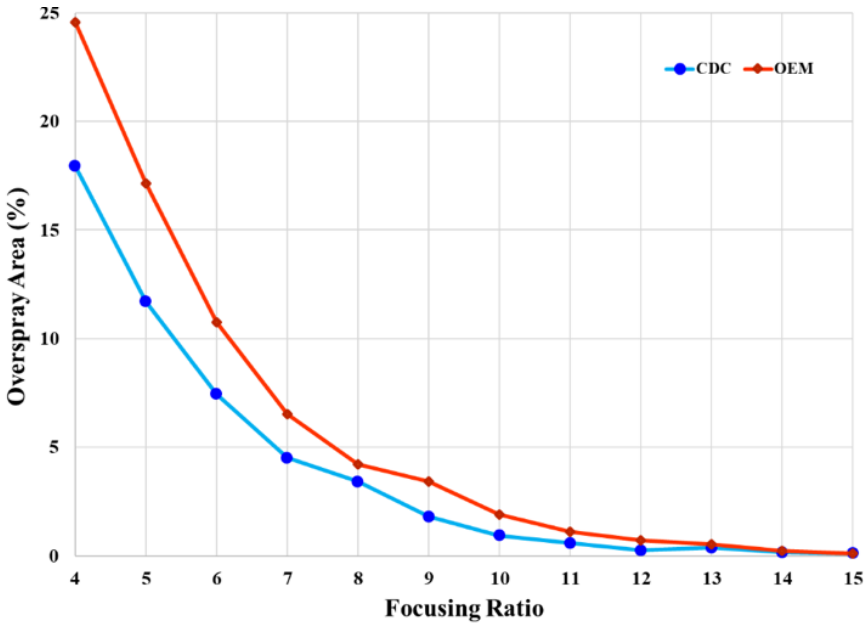

Figure 7. Percent area coverage due to overspray versus focusing ratio with fixed CGFR 10 and stand-off distance 1.25mm.

4.4. Resistivity Measurements

The resistivity analysis of the printed circuits, as shown in Figure 8A, demonstrated comparable performance between the 22G tapered tip nozzle, shown in Figure 8B, and the SLA-manufactured multi-throat CD micro-nozzle, depicted in Figure 8C. The resistance of the circuit printed with the 22G tapered tip nozzle was $172 \pm 18.04\ \Omega$, while the resistance of the printed circuit with the multi-throat CD micro-nozzle was $156 \pm 7.68\ \Omega$. The resistivity of the circuit printed with the multi-throat CD micro-nozzle was slightly higher at $1.57 \times 10^{-5}\ \Omega$m than compared to $1.42 \times 10^{-5}\ \Omega$m for an identical circuit manufactured with a 22G commercial nozzle. This indicates that the SLA-printed nozzles can produce functional circuits with performance comparable to those made with commercial nozzles.

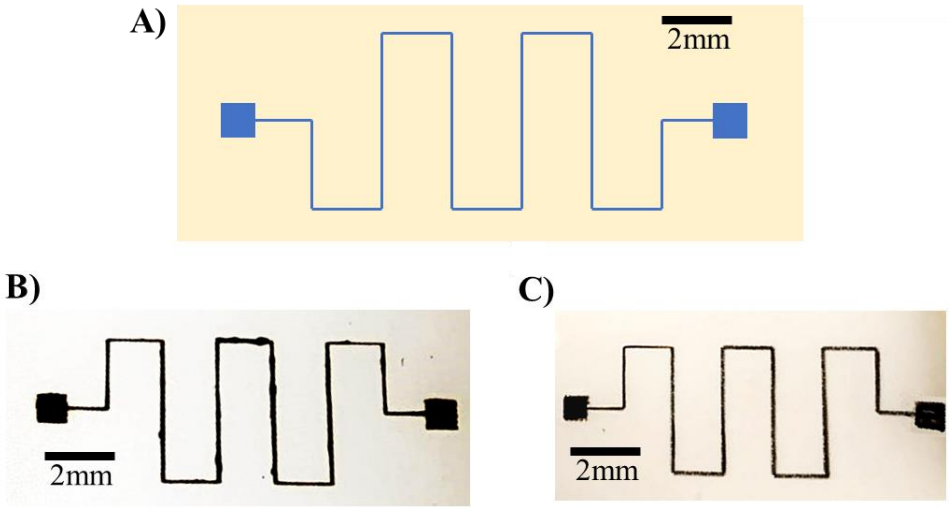

Figure 8. (A) Designed circuit; (B) Circuit printed with the 22G tapered tip nozzle after sintering, and (C) Circuit printed with the SLA-printed multi-throat CD micro-nozzle printed circuit after sintering. Scale bar, 2 mm.

5. Conclusions

This study demonstrates an advancement in the AJP process by reducing overspray and improving print resolution by integrating converging-diverging sections into an SLA-printed micro-nozzle. Numerical simulations and experimental tests both were conducted to compare the performance of the CD nozzle with a standard 22G tapered tip OEM nozzle. The results suggest the following conclusions:

- The CD micro nozzle reduced overspray compared to the OEM nozzle, with overspray percentages decreasing by 17.821% at a low focusing ratio of 4. However, both nozzles show minimal overspray at higher focusing ratios (14-15).
- CFD simulations predicted that the CD nozzle contributes to a higher aerosol exit velocity and narrower line widths compared to the OEM nozzle. Although the actual printed line widths were slightly wider than CFD predicted due to unaccounted ink-substrate interactions, the CD micro nozzle consistently outperformed the OEM nozzle in producing finer lines.
- The resistivity of circuits printed with the CD micro nozzle was slightly higher than those printed with the OEM nozzle. However, the resistance values were comparable, indicating that the CD micro nozzle can produce functional electronic circuits with similar performance to those made with commercial nozzles.

6. Limitations and Future Work

A few simplified assumptions were made to facilitate our analysis for this pilot study. First, our analysis assumed monodisperse aerosol droplets (3 μm), assuming a uniform particle size distribution, while practical applications often involve polydisperse droplets. In addition, the stand-off distance between the nozzle and the substrate was fixed at 1.25 mm, although aerosol deposition characteristics varied significantly with different stand-off distances. In addition, we assumed a particle trap condition and neglected interactions between aerosol droplets and the substrate. Finally, only one version of the multi-throat nozzle was evaluated, and the design and dimensions of the nozzle have not yet been subjected to optimization studies.

References

[1] H. Kim, Y. S. Kim, and W. H. Yeo, "3 - Aerosol jet printing toward advanced electronics: Versatile, facile, additive processes for 2D/3D structuring," in *Smart and Connected Wearable Electronics*, W.-H. Yeo and Y.-S. Kim, Eds., in Woodhead Publishing Series in Electronic and Optical Materials. , Woodhead Publishing, 2024, pp. 97–121. doi: 10.1016/B978-0-323-99147-6.00001-6.

[2] C. H. Rao, K. Avinash, B. K. S. V. L. Varaprasad, and S. Goel, "A Review on Printed Electronics with Digital 3D Printing: Fabrication Techniques, Materials, Challenges and Future Opportunities," *J. Electron. Mater.*, vol. 51, no. 6, pp. 2747–2765, Jun. 2022, doi: 10.1007/s11664-022-09579-7.

[3] J. Q. Feng and M. J. Renn, "Aerosol Jet® Direct-Write for Microscale Additive Manufacturing," *J. Micro Nano-Manuf.*, vol. 7, no. 1, p. 011004, Mar. 2019, doi: 10.1115/1.4043595.

[4] P. V. Arsenov, A. A. Efimov, and V. V. Ivanov, "Optimizing Aerosol Jet Printing Process of Platinum Ink for High-Resolution Conductive Microstructures on Ceramic and Polymer Substrates," *Polymers*, vol. 13, no. 6, Art. no. 6, Jan. 2021, doi: 10.3390/polym13060918.

[5] G. Gramlich, R. Huber, F. Häslich, A. Bhutani, U. Lemmer, and T. Zwick, "Process considerations for Aerosol-Jet printing of ultra fine features," *Flex. Print. Electron.*, vol. 8, no. 3, p. 035002, Sep. 2023, doi: 10.1088/2058-8585/ace3d8.
[6] S. Ramesh *et al.*, "Numerical and experimental investigation of aerosol jet printing," *Addit. Manuf.*, vol. 59, p. 103090, Nov. 2022, doi: 10.1016/j.addma.2022.103090.
[7] N. Dalal, Y. Gu, G. Chen, D. R. Hines, A. Dasgupta, and S. Das, "Effect of Gas Flow Rates on Quality of Aerosol Jet Printed Traces With Nanoparticle Conducting Ink," *J. Electron. Packag.*, vol. 142, no. 011012, Nov. 2019, doi: 10.1115/1.4044960.
[8] M. Smith, Y. S. Choi, C. Boughey, and S. Kar-Narayan, "Controlling and assessing the quality of aerosol jet printed features for large area and flexible electronics," *Flex. Print. Electron.*, vol. 2, no. 1, p. 015004, Feb. 2017, doi: 10.1088/2058-8585/aa5af9.
[9] S. Ramesh, Z. Xu, I. V. Rivero, and D. R. Cormier, "Computational fluid dynamics and experimental validation of aerosol jet printing with multi-stage flow focusing lenses," *J. Manuf. Process.*, vol. 95, pp. 312–329, Jun. 2023, doi: 10.1016/j.jmapro.2023.03.035.
[10] P. Lall, A. Abrol, N. Kothari, B. Leever, and S. Miller, "Process Capability of Aerosol-Jet Additive Processes for Long-Runs Up to 10-Hours," *J. Electron. Packag.*, vol. 142, no. 041003, Oct. 2020, doi: 10.1115/1.4048535.
[11] G. Tarabella, D. Vurro, S. Lai, P. D'Angelo, L. Ascari, and S. Iannotta, "Aerosol jet printing of PEDOT:PSS for large area flexible electronics," *Flex. Print. Electron.*, vol. 5, no. 1, p. 014005, Jan. 2020, doi: 10.1088/2058-8585/ab61c4.
[12] R. R. Tafoya and E. B. Secor, "Understanding effects of printhead geometry in aerosol jet printing," *Flex. Print. Electron.*, vol. 5, no. 3, p. 035004, Jul. 2020, doi: 10.1088/2058-8585/aba2bb.
[13] S. Bhattacharya, A. Lutfurakhmanov, J. M. Hoey, O. F. Swenson, Z. Mahmud, and I. S. Akhatov, "Aerosol Flow Through a Converging-Diverging Micro-Nozzle," *Nonlinear Eng.*, vol. 2, no. 3–4, Jan. 2013, doi: 10.1515/nleng-2013-0020.
[14] Y. Akedo *et al.*, "Effect of Convergent-Divergent Nozzle on Fine Particle Velocity in Low-Pressure Induction Plasma Jet in Plasma-Assisted Aerosol Deposition," *Plasma Chem. Plasma Process.*, vol. 44, no. 1, pp. 583–600, Jan. 2024, doi: 10.1007/s11090-023-10361-8.
[15] L. Alonso, M. A. Garrido, and P. Poza, "An optimisation method for the cold-spray process: On the nozzle geometry," *Mater. Des.*, vol. 214, p. 110387, Feb. 2022, doi: 10.1016/j.matdes.2022.110387.
[16] L. Meng, W. Wang, B. Xu, J. Qin, K. Zhang, and H. Liu, "Solution-Processed Flexible Transparent Electrodes for Printable Electronics," *ACS Nano*, vol. 17, no. 5, pp. 4180–4192, Mar. 2023, doi: 10.1021/acsnano.2c10999.
[17] T.-R. Lv *et al.*, "Micro/Nano-Fabrication of Flexible Poly(3,4-Ethylenedioxythiophene)-Based Conductive Films for High-Performance Microdevices," *Small*, vol. 19, no. 30, p. 2301071, 2023, doi: 10.1002/smll.202301071.
[18] X. Xu, Y. Zhao, and Y. Liu, "Wearable Electronics Based on Stretchable Organic Semiconductors," *Small*, vol. 19, no. 20, p. 2206309, 2023, doi: 10.1002/smll.202206309.
[19] M. Galloway, S. Hin Lam, H. Amel, R. Richardson, R. Kay, and M. Jabbari, "Implementation of nozzle motion for material extrusion additive manufacturing in Ansys Fluent," *Virtual Phys. Prototyp.*, vol. 19, no. 1, p. e2397816, Dec. 2024, doi: 10.1080/17452759.2024.2397816.

[20] B. Fox, K. C.-H. Wu, S. Ma, and S. Y. M. Wan, "A CFD simulation platform for surface finishing processes in advanced manufacturing," *Adv. Eng. Softw.*, vol. 196, p. 103716, Oct. 2024, doi: 10.1016/j.advengsoft.2024.103716.

[21] E. Ramon *et al.*, "Large-scale fabrication of all-inkjet-printed resistors and WORM memories on flexible polymer films with high yield and stability," *Flex. Print. Electron.*, vol. 6, no. 1, p. 015003, Jan. 2021, doi: 10.1088/2058-8585/abdb40.